catalysts

MDPI

Article

MnO_2 Doped with Ag Nanoparticles and Their Applications in Antimicrobial and Photocatalytic Reactions

G. Anguraj [1], R. Ashok Kumar [1,*], C. Inmozhi [2], R. Uthrakumar [3], Mohamed S. Elshikh [4], Saeedah Musaed Almutairi [4] and K. Kaviyarasu [4,5,6,*]

1 Department of Physics, Thiruvalluvar Government Arts College, Rasipuram 637401, Tamil Nadu, India
2 Department of Physics, Government Arts College for Women, Salem 636008, Tamil Nadu, India
3 Department of Physics, Government Arts College (Autonomous), Salem 636007, Tamil Nadu, India
4 Department of Botany and Microbiology, College of Science, King Saud University, P.O. Box 2455, Riyadh 11451, Saudi Arabia
5 UNESCO-UNISA Africa Chair in Nanosciences/Nanotechnology Laboratories, College of Graduate Studies, University of South Africa (UNISA), Muckleneuk Ridge, Pretoria P.O. Box 392, South Africa
6 Nanosciences African Network (NANOAFNET), Materials Research Group (MRG), iThemba LABS-National Research Foundation (NRF), 1 Old Faure Road, 7129, Somerset West P.O. Box 722, Western Cape Province, South Africa
* Correspondence: author: rajamaniashokkumar@gmail.com (R.A.K.); kavi@tlabs.ac.za (K.K.)

Abstract: A wide range of nanoparticles have been produced for photocatalysis applications. Nonetheless, degrading organic dyes requires nanoparticles that are efficient and excellent. As a photocatalyst, pure manganese oxide (MnO_2) was prepared via a sol–gel method using silver (Ag) nanoparticles of transition metal oxide. In addition to X-ray diffraction (XRD), scanning electron microscopy (SEM), and energy dispersive X-ray spectroscopy (EDX), the crystal structure and elemental composition were analysed. According to XRD data, the transition metal of MnO_2 oxide is highly pure and has a small crystallite size. The presence of functional groups was confirmed and clarified using Fourier-transform infrared spectra (FTIR). By irradiating the transition pure and doped MnO_2 photocatalysts with visible light, the UV-vis, μ-Raman, and surface areas were determined. As a result, of using the photocatalysts with aqueous methylene blue (MB) solutions under visible light irradiation, the MnO_2 doped with Ag nanoparticles demonstrated high degradation efficiencies and were utilised to establish heterogeneous photocatalysis dominance. In this paper, we demonstrate that the photocatalytic efficiency of transition metal oxides is exclusively determined by the particle size and surface area of nano-sized materials. Due to their high surface charge ratio and different surface orientations, have the highest photocatalytic efficiency. Generally, MnO_2 doped with Ag nanoparticles is resistant to bacteria of both *Gram-positive* and *Gram-negative* types (*B. sublittus* and *Escherichia coli*). There is still a need for more research to be performed on reducing the toxicity of metal and metal oxide nanoparticles so that they can be used as an effective alternative to antibiotics and disinfectants, particularly for biomedical applications.

Keywords: manganese oxide (MnO_2); silver nanoparticles; sol–gel method; photocatalysis behaviour; wastewater treatment; antimicrobial activity

check for updates

Citation: Anguraj, G.; Ashok Kumar, R.; Inmozhi, C.; Uthrakumar, R.; Elshikh, M.S.; Almutairi, S.M.; Kaviyarasu, K. MnO_2 Doped with Ag Nanoparticles and Their Applications in Antimicrobial and Photocatalytic Reactions. *Catalysts* **2023**, *13*, 397. https://doi.org/10.3390/catal13020397

Academic Editors: Farid Orudzhev and Irina A. Zvereva

Received: 27 September 2022
Revised: 17 January 2023
Accepted: 9 February 2023
Published: 12 February 2023

Copyright: © 2023 by the authors. Licensee MDPI, Basel, Switzerland. This article is an open access article distributed under the terms and conditions of the Creative Commons Attribution (CC BY) license (https://creativecommons.org/licenses/by/4.0/).

1. Introduction

As the century progresses, environmental degradation will become more and more prevalent. There is an increase in both the variety and quantity of pollutants, from nuclear waste to microplastics. As we move into the new era of science and technology, nanoparticles have indeed proven the ability of researchers to harness the *'science of small'* to achieve greater industrial revolutions, especially in the area of electronics. In all spheres of life, it has a positive impact on every aspect of life due to its significant global market share and salutary impact [1]. When particles are reduced to the nano scale, their properties change

drastically, both physically and chemically. By controlling the properties of materials at the nanoscale level rather than by changing their composition, new techniques are being developed to control the properties of materials. Due to their distinct optical and chemical properties, semiconductor nanoparticles have attracted much attention in recent years due to their exciting properties, including tunable bandgaps as a function of size, nonlinear optical properties, and luminescence [2]. As a result, these nanoparticles are suitable for a wide range of electronic applications, such as sensors, photocatalytic reactions, and optoelectronic devices.

In the environment we live in, there are many pollutants, such as alcohols, carboxylic acids, amines, herbicides, and aldehydes, that can be degraded with great efficiency by photocatalysis. Photocatalysis is a novel approach and a requisite tool that exhibits high-efficiency degradation of pollutants. Semiconductor nanoparticles play a significant role as photocatalysts, since their enhanced properties enable them to destroy pollutants through chemical reaction [3]. Thus, tuning the morphology of nanomaterials requires understanding of their growth process and parameters. In recent years, semiconductor nanoparticles have attracted much more attention due to their quantum confinement effect, since researchers across the globe are working on this in order to create a sustainable future. As a result of strong interactions between hole–electron (e-/h+) pairs generated by excited photons, semiconductors might exhibit quantum confinement effects when the size of the nanoparticles exceeds the Bohr radius exciton [4]. In biomedical sciences, the synthesis of transition metal and metal oxide nanoparticles is becoming more prominent [5]. Metal oxide-linked semiconductor photocatalysts have attracted a lot of press regarding their usage in environmental remediation, where they are utilised degrade contaminants in the air and water [6]. Coloured wastewater results in ecological effects, caused by increasing concentrations of dyes are substances with a wide range of applications, primarily for colouring the final products of textiles, precious stones, leather, paper, plastics, and food [7]. For years, semiconductor photocatalysts have been used to remove organic and inorganic pollutants from water. Regardless, many photocatalysts have been created, because of their better stability, non-toxicity, and antibacterial qualities, metal oxide semiconductors have attracted a lot of interest [8]. The quantum confinement effect causes the bulk properties of the particles to vanish as the particle size is lowered, and fresh features emerge because of the quantum confinement effect. Nanomaterials possess different characteristics with respect to size, structure, surface orientations, degradation efficiency and bacterial activity [9,10]. The high surface area-to-volume ratio of the particle improves as the particle size is lowered, resulting in improved attributes such as enhanced catalytic and antibacterial activities. Various metal oxide nanoparticles, such as MnO_2 doped with Ag nanoparticles, have attained remarkable growth in recent years [11,12]. The optical, catalytic, mechanical, and antibacterial applications of MnO_2 nanoparticles are driving intense research activity.

Wastewater treatment, solar energy conversion, dye degradation electronics, and catalysis are just a few of the applications for transition metal oxides [13–17]. Because of their non-toxicity, low cost, abundance, durability in aquatic environments, and modest bandgap of 2.0–2.2 eV, the metal oxide nanoparticles have particular interest among these oxide nanoparticles. The small bandgap of metal oxide makes the materials are suitable for photoconductive and photothermal applications. MnO_2 has also been employed in medicine delivery, biosensors, energy devices, photocatalysis, and antimicrobial applications in printed electronics [18–22]. Metal oxide nanoparticles are synthesised for antimicrobial uses, such as medicinal treatments, industry production, and widespread absorption into varied materials, such as cosmetics and apparel, are currently gaining popularity. Generally, metals of similar size to the parent ion provide effective property enhancement without significantly altering structural qualities. When different transition metals are doped into oxide nanoparticles, similar alterations have been found. Due to their low bandgap, chemical stability, and inertness, metal oxide semiconductor nanocrystals such as TiO_2, ZnO, MgO, WO_3, MnO_2, and SnO_2 have recently acquired favour as photocatalysts [23–26]. The use of metal ion doping in MnO_2 to achieve visible-range absorbance has been investigated.

Another advantage of doping MnO_2 with metal ions in the correct amounts is reduced antibacterial energy transfer. Its chemical interactions, in particular, are responsible for various pharmacological and antibacterial activities.

We produced nanoparticles using the sol–gel process and explained their properties. X-ray diffraction (XRD) analysis, UV-vis absorbance spectroscopy, FTIR, μ-Raman spectroscopy, scanning electron microscopy (SEM), energy dispersive X-ray spectroscopy (EDS), and photocatalytic activity have all been described. As far as we know, no paper has been published on the antibacterial activity of MnO_2 doped with Ag nanoparticles. These investigations focus on changes in the crystalline structure, surface morphology, antibacterial activity, and photocatalytic activity of MnO_2 on methylene blue as photocatalysts for biological and environmental applications were reported in detail.

2. Results and Discussion

2.1. XRD Analysis

The rhombohedral (hexagonal) structure of hematite presents twelve pronounced peaks with crystal planes of (200), (202), (300), (211), (330), (301), and (321). Since the amount of Ag dopant in the produced compounds is so tiny, no phase matching to silver nanoparticles or other silver samples can be seen in the XRD pattern, indicating that silver centres are lodged in the MnO_2 lattice, as shown in Figure 1. The Debye–Scherrer expression can also be used to compute the crystallite size of synthetic substances from results, also corroborating these findings. Stiff narrow peaks without any notable shift indicate that the nanoparticle products were observed upon evaluation of MnO_2 doped with Ag nanoparticles under X-ray diffraction, signifying that the particles were pure, with a = ~89.83 nm; the crystallite size was determined using Debye–Scherrer equation, $D = K\lambda/\beta cos\theta$, where D represents the crystallite size, K represents the Scherrer constant (0.9), presents the X-ray wavelength, represents the full width at half maximum (FWHM), and represents the diffraction angle. The lattice parameters (a = b and c for a hexagonal unit cell) were determined using the following equation [27–29].

$$\frac{1}{d_{hkl}} = \frac{4}{3} \cdot \frac{h^2 + k^2 + l^2}{a^2 + b^2 + c^2} \quad (1)$$

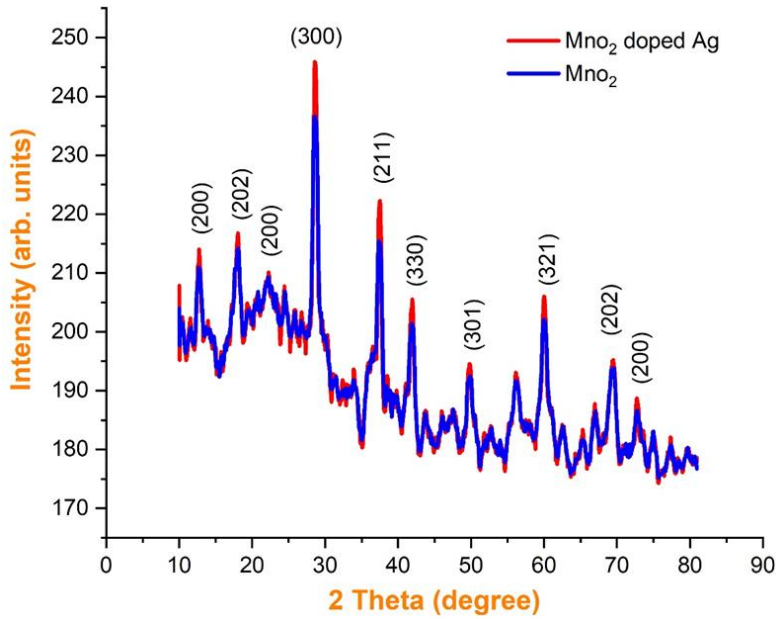


Figure 1. X-ray diffraction pattern of pure MnO_2 and MnO_2 doped with Ag nanoparticles.

The inter-reticular distance is d_{hkl}, the lattice parameters are a, b and c, and the Miller indices are h, k, and l. For pure MnO_2 and MnO_2 doped with Ag nanoparticles, average crystalline sizes of 14 nm and 20.77 nm, respectively, were computed [30–32].

2.2. UV Absorbance Analysis

By recording the UV-visible absorbance spectrum of nanomaterial suspensions, the optical bandgap was estimated. Using the UV-vis spectra, the *Tauc-plot* relation was then employed to establish bandgaps. The absorption coefficient (α) is given by $h\nu = (h\nu - E_g)^m$ according to the *Tauc relation*, $\alpha h\nu = \beta\ (h\upsilon - E_g)^m$; where β is a constant with variable values for different transitions, E_g is the bandgap energy, h is the energy of a photon, and m is an exponent with varying weights depending on the electronic change [33–35]. All samples were evaluated in the UV-vis region of 200 nm to 600 nm. Optical analysis was performed using a dual-beam 60 UV-visible NIR spectrophotometer. Figure 2 shows the absorption spectrum of bare manganese oxide (MnO_2) and MnO_2 doped with Ag nanoparticles, with absorption at 311 nm are confined in bare MnO_2 is due to charge transfer of ions and absorption band obtained at 324 nm are found in MnO_2 doped with Ag nanoparticles, which explains charge transfer via direct ligand-to-metal transition in the optical absorption spectrum. The straight bandgaps of pure MnO_2 and MnO_2 doped with Ag nanoparticles were 2.79 eV and 2.66 eV, respectively, as shown in Figure 3.

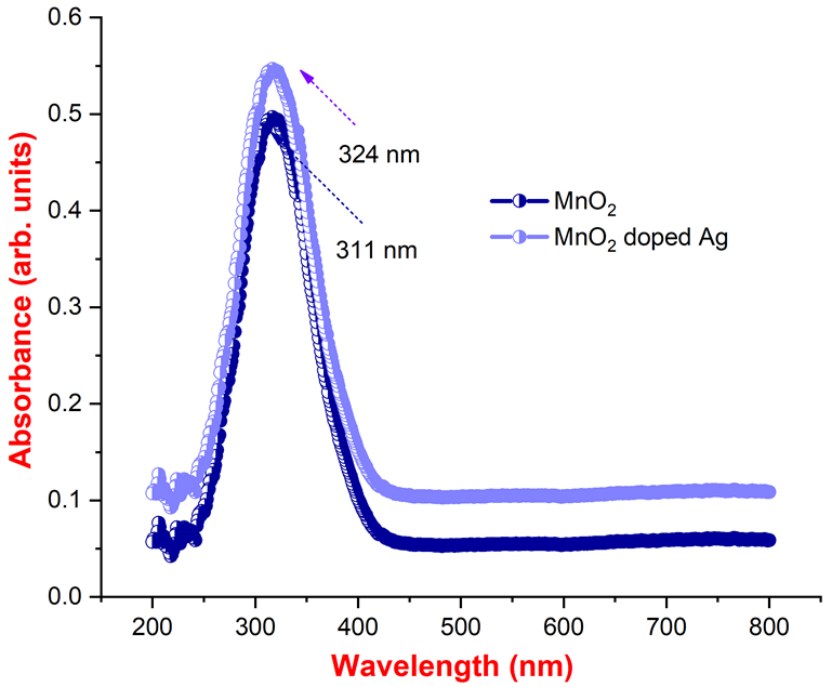


Figure 2. UV-visible spectrum of synthesised pure MnO_2 and MnO_2 doped with Ag nanoparticles.

2.3. FTIR Analysis

The FTIR spectra were collected in the 4000–500 cm^{-1} range. The FTIR spectra of pure MnO_2 and MnO_2 doped with Ag nanoparticles are shown in Figure 4. Significant peaks can be observed at 3366 cm^{-1}, 2359 cm^{-1}, 1611 cm^{-1}, 1122 cm^{-1}, 641 cm^{-1} and 515 cm^{-1}. The stretching mode of the -OH group corresponds to a broad band at 3366 cm^{-1}. The H-O-H bending vibration of water contained in moisture received from the atmosphere is allocated to a bar near 1611 cm^{-1}. Ag ions may be responsible for the bands at 1478 cm^{-1}. The distinctive absorption of Mn-O stretching at around 641 cm^{-1} indicates the establishment of Mn-O bonds in the produced nanomaterials. The FTIR spectra of doped metal oxide nanoparticles are also shown in Figure 4. The curves contain comparable peaks, with the Mn-O rise shifting to 515 cm^{-1}. On doping, the strength of the Mn-O height

was similarly reduced. This modest shift in band validates doping in nanomaterials, but lower intensity indicates minimal doping and causes a minor skeletal perturbation in the Mn-O structure [36]. This decline is easily explained by Hook's law, which asserts that the vibration frequency is indirectly proportional to mass reduction, with the vibrational frequency shifting to a lower value with increasing condensed mass.

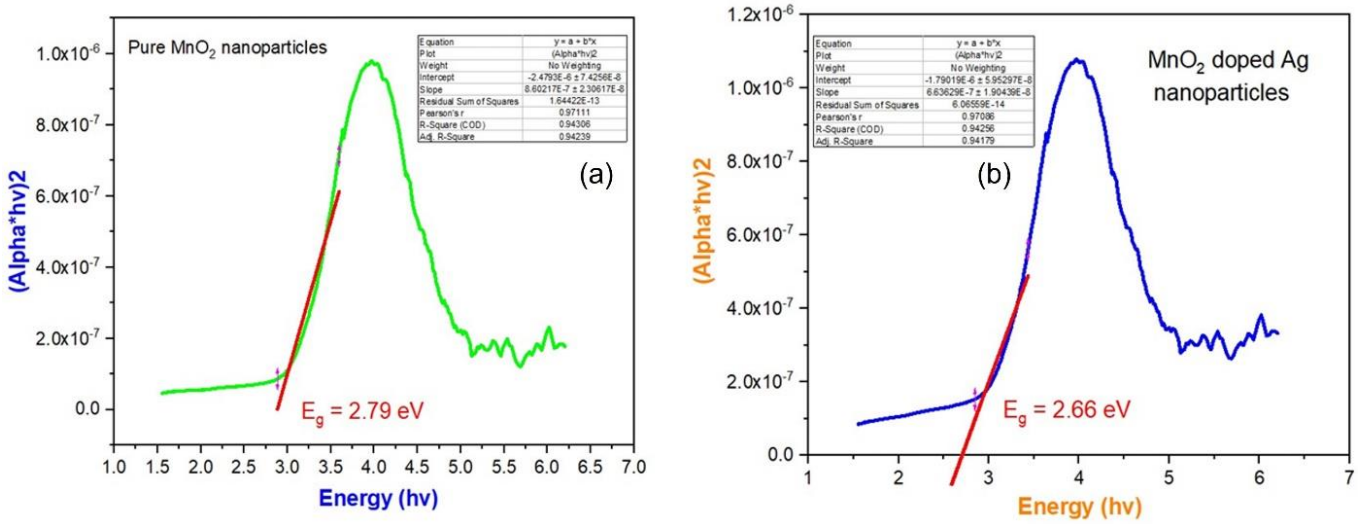


Figure 3. *Tauc-plot* relation spectrum of synthesised (**a**) pure MnO_2 and (**b**) MnO_2 doped with Ag nanoparticles.

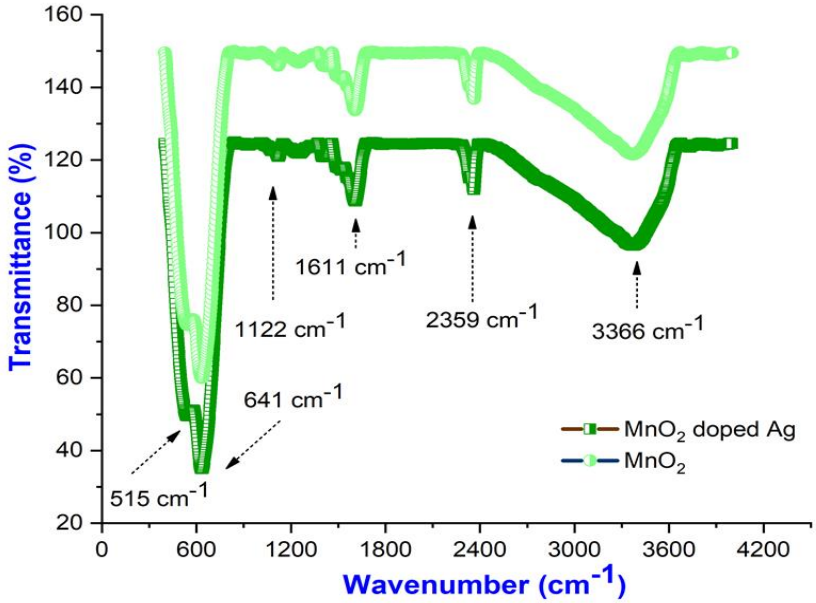


Figure 4. FTIR spectrum of synthesised pure MnO_2 and MnO_2 doped with Ag nanoparticles.

2.4. Scanning Electron Microscopy and EDX Analysis

The particle grains of MnO_2 nanoparticles of a few nanometres are presented in Figure 5a,b, indicating that pure nanostructures and those doped with Ag were successfully synthesised, as reported in Figure 5c,d. Due to the increased density and reduction in grain size with doping, the smaller nanoparticles are visible and less agglomerated in the SEM image of MnO_2 doped with Ag nanoparticles, resulting in a large surface area that is ideal for photocatalytic activity. It is also evident that the MnO_2 particles formed in nature are porous and have a grain size of roughly 24 nm [37–39]. The elemental compositions

of the generated distinct samples are also confirmed using EDX, and their spectra are presented in the EDX spectrum for pure and doped MnO_2, respectively. Mn, Ag, and O components are visible in the EDX spectrum. The concentration of Ag in the doped samples is determined to be 4.29 percent. The chemical compositions of Mn and O in pure Mn-O_2 nanoparticles are 54.66% and 42.37%, respectively, as shown in Figure 5e. The iron proportion in MnO_2 doped Ag nanoparticles, on the other hand, fell, while the oxygen percentage increased somewhat [40].

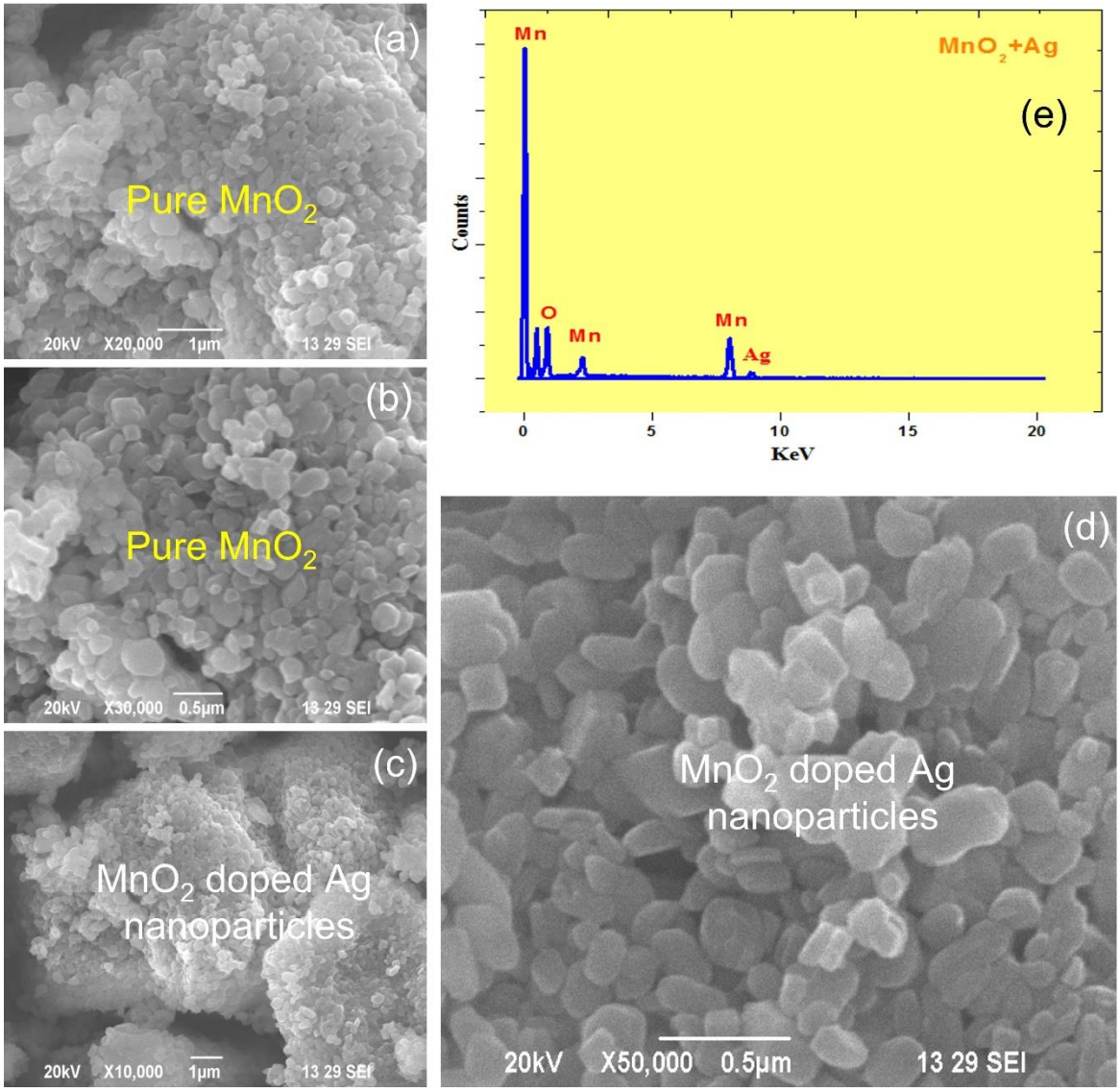


Figure 5. (**a**–**e**) Scanning electron microscopy images of (**a**–**b**) pure MnO_2; (**c**–**d**) MnO_2 doped with Ag nanoparticles; and EDX spectrum (**e**).

2.5. Raman Spectroscopy

Raman spectroscopy is a powerful technique for investigating complex structures and chemical bonds. Figure 6 depicts the creation of a rhombohedral phase constructed of pure MnO_2 and MnO_2 doped with Ag nanoparticles, as revealed by Raman analysis. The Mn, Ag and O stretching vibrational modes of metal–oxygen interaction between Mn and O atoms are responsible for three significant peaks at 74 cm^{-1}, 437 cm^{-1}, and 1054 cm^{-1} in MnO_2 nanoparticles treated by a simple sol–gel process. The Ag and Mn-O modes of MnO_2 nanoparticles produce a couple of soft peaks at 940 cm^{-1} and 1427 cm^{-1}. The production of MnO_2 nanoparticles is responsible for the substantial high-intensity

rise at 1054 cm^{-1} [41–43]. The Raman peak intensities and peak positions match the face-centred MnO_2 doped with Ag nanoparticles, as previously reported [44–46].

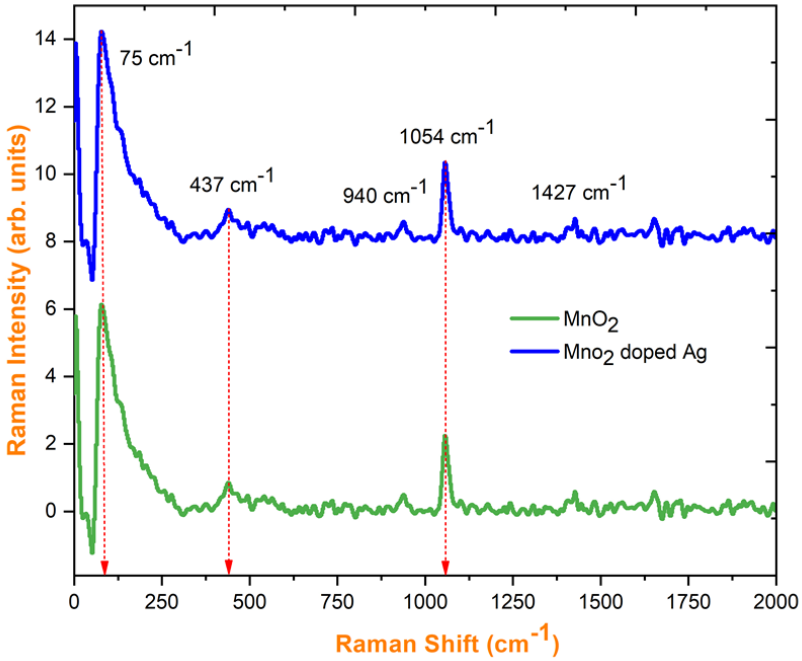


Figure 6. Raman spectrum of synthesised pure MnO_2 and MnO_2 doped with Ag nanoparticles.

2.6. Photocatalytic Analysis

In photodegradation reactions, the intensity of incident light, the beginning concentration of pollutants, and the concentration of the photocatalyst are all significant characteristics. Two main approaches are important during photocatalytic experiments in the presence of transition metal ions: (a) the effect of transition metal ions on photocatalysis reaction rate, and (b) the concentration of metal ions into less toxic species or the deposition of ions on catalyst surface to recover the expensive and useful metal ions. A photocatalysis experiment was performed on generated all transition metal oxide nanoparticle samples [47,48]. Methylene blue (MB), an organic dye, was used to track the performance of photocatalysis. The solution was placed in the dark to maintain adsorption and desorption equilibrium at room temperature after 50 mm of 5 ppm MB solution and 2 mg of catalyst were dissolved. After defined intervals of time (0, 30, 60, 90, 120, min), the rate of absorption was measured using a Carry 60 UV-visible spectrophotometer.

$$\text{Degradation} = \eta = [1 - C_o/C_t] \times 100 \quad (2)$$

The relation given above was used to calculate the percentage of methylene blue degradation. Photo-degradation of metal oxides MnO2 is depicted in Figure 7a–b. With time, the distinct colour of organic dye (MB) faded. Methylene blue's transparent hue indicates that the dye has completely degraded. Figure 8 shows the degradation rate of nano-photocatalysts made from various cycles. The reactions throughout the experiment follow pseudo-first-order kinetics, as seen in the graphs. The simple oxides exhibited good catalytic activity, as evidenced by degradation percentages and rate constant values of distinct transition metal oxides. The formation of excitations on UV visible light exposure is required for the photocatalytic activities of transition metal oxides. When a photocatalyst is subjected to UV-vis light, electrons from the valence band are stimulated to the conduction band, and electron–hole pairs are formed. The resulting pairs can recombine or interact with other molecules [49]. To precede oxidation–reduction processes, electron–hole pairs at CB and VB migrate towards the photocatalyst surface, which immediately interacts

with the dye solution. The degradation efficiency of the synthesised MnO_2 doped with Ag nanomaterials was found to be 90%, meaning that the material can employed as an excellent photocatalyst. Figure 9 shows the reaction mechanism occurring during the photocatalytic activity of the MnO_2 doped with Ag nanoparticle photocatalyst under visible light.

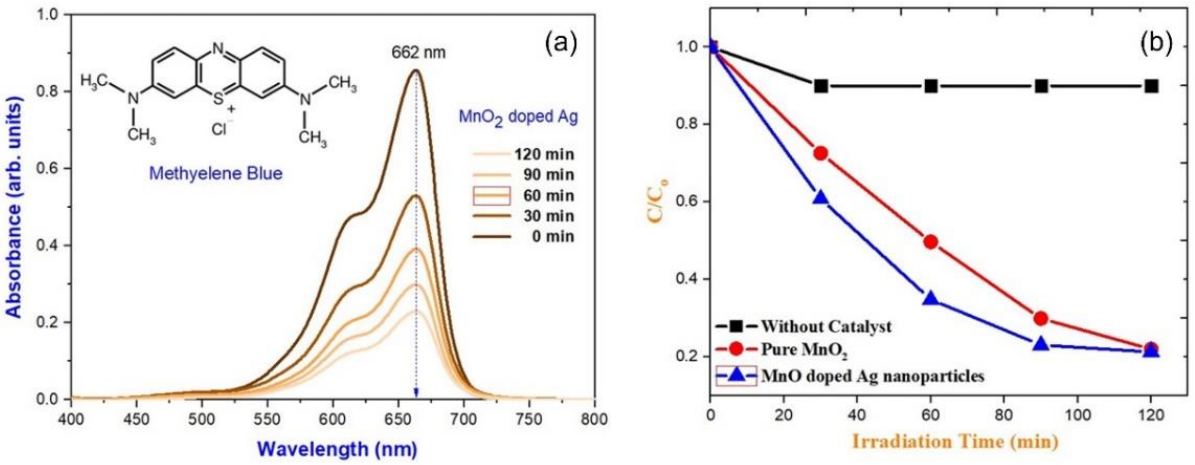


Figure 7. (**a**) UV-vis absorption spectrum of MB recorded and (**b**) the plot of C/C_o vs. time for the degradation in the presence of MnO_2 doped with Ag nanoparticles.

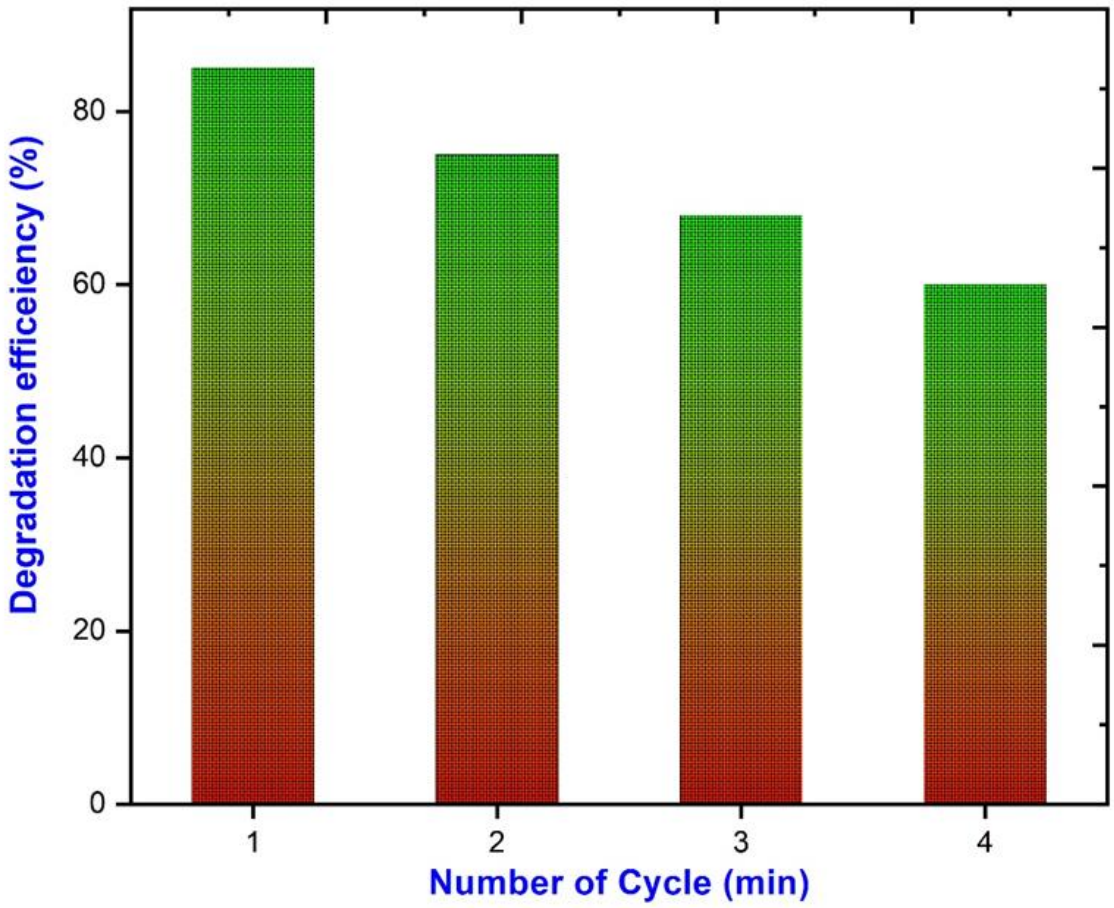


Figure 8. Photocatalytic degradation efficiency bar diagram of MnO_2 doped with Ag nanoparticles.

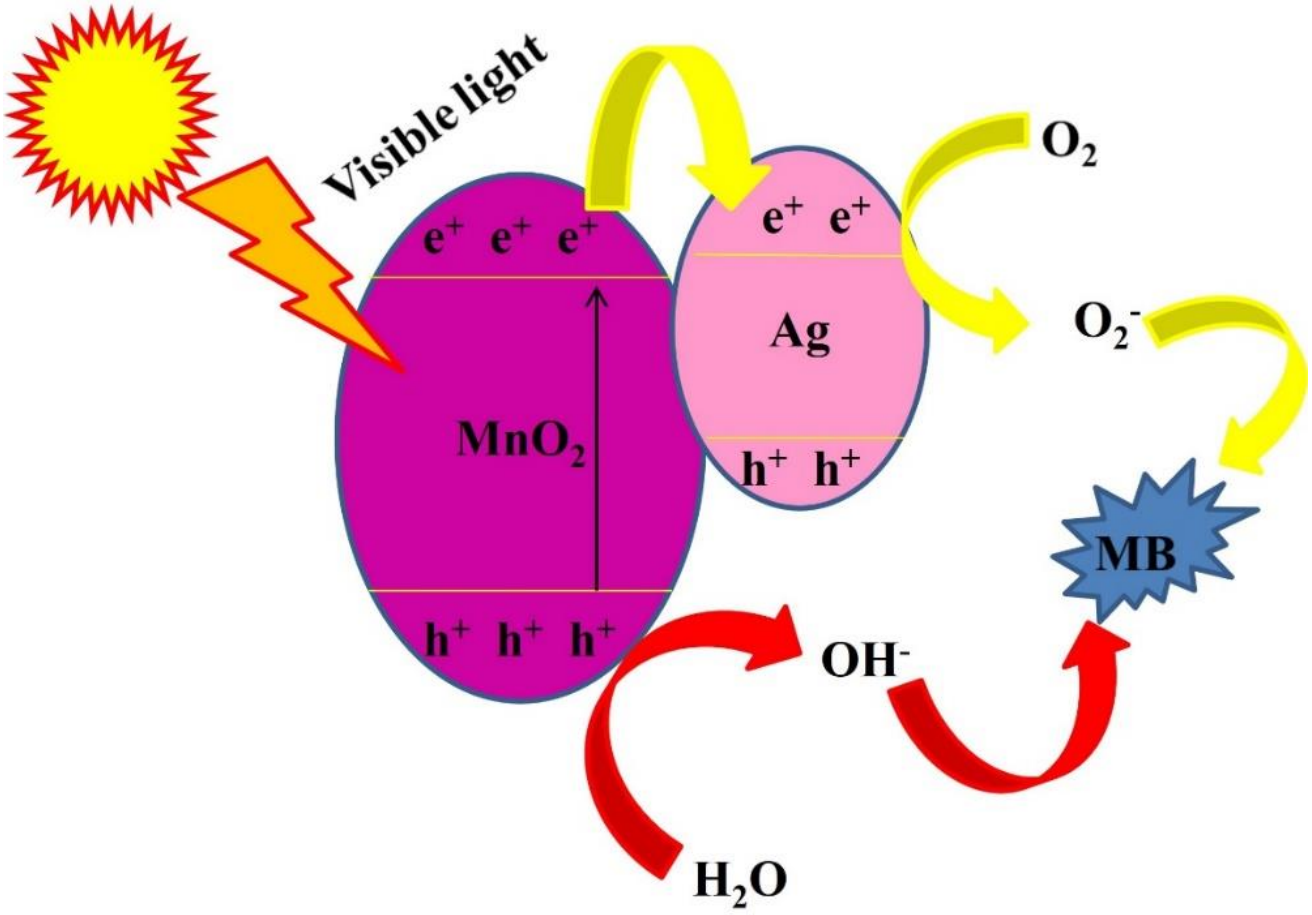


Figure 9. A proposed mechanism for photocatalytic reaction with MnO_2 doped with Ag nanoparticles.

2.7. Screening of Antibacterial Activity

Two bacterial strains (*Bacillus subtilis* and *Escherichia coli*) were used throughout the investigation. All the bacterial cultures were obtained from the microbial type culture collection (MTCC), institute of microbial technology, Chandigarh, India. The young bacterial broth cultures were prepared before the screening procedure as follows: (i) preparation of inoculums: stock cultures were maintained at 4 °C on slopes of nutrient agar. Active cultures were prepared for the experiment by transferring a loopful of cells from the stock cultures to test tube of Muller–Hinton broth (MHB) for bacteria that were incubated without agitation for 24 h at 37 °C and 25 °C, respectively. The cultures were diluted with fresh Muller–Hinton broth to achieve optical densities corresponding to 2.0×10^6 colony forming units (CFU/mL) for bacteria.

2.7.1. Antimicrobial Susceptibility Test

The disc diffusion method was used to screen the antimicrobial activity. In vitro antimicrobial activity was screened by using Muller–Hinton Agar (MHA) obtained from Himedia (Mumbai). The MHA plates were prepared by pouring 15 mL of molten media into sterile petriplates. The plates were allowed to solidify for 5 min, and 0.1% inoculum suspension was swabbed uniformly, and the inoculums were allowed to dry for 5 min. The concentration of extracts is 40 mg/disc was loaded on a 6 mm sterile disc. The loaded disc was placed on the surface of medium and the extract was made it possible to diffuse for 5 min, and the plates were kept for incubation at 37 °C for 24 h. At the end of incubation, inhibition zones formed around the disc were measured with transparent ruler in millimetres is shown in Figure 10a,b. Antibacterial activity of Ag nanoparticles was seen at ultra-low concentrations; however, the antibacterial activity of MnO_2 nanoparticles was

dependent on concentration and surface area. The antibacterial activity of pure and doped MnO_2 nanoparticles against Gram-negative bacteria (*E. coli*) and Staphylococcus aureus was examined. The zones of inhibition of MnO_2 doped with Ag nanoparticles against Gram-positive and Gram-negative bacteria strains are shown in Figure 11a,b. The materials are viewed at the impact of particle size reduction and concentration on the antibacterial activity of MnO_2 nanoparticles. The antibacterial activity of MnO_2 nanoparticles improved significantly with increasing Ag powder content, according to our findings [50,51].

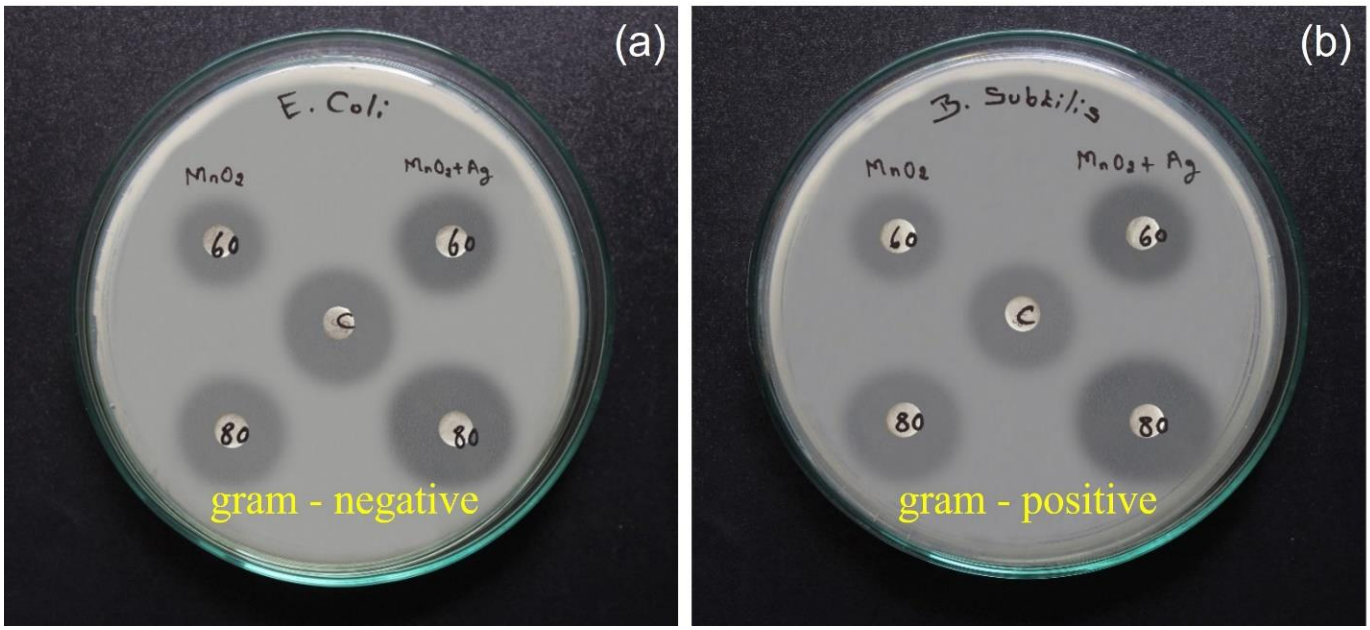


Figure 10. (**a**,**b**). Antibacterial activity of MnO_2 doped with Ag nanoparticles against Gram-negative (*Escherichia Coli*) and Gram-positive (*Bacillus subtilis*) strains.

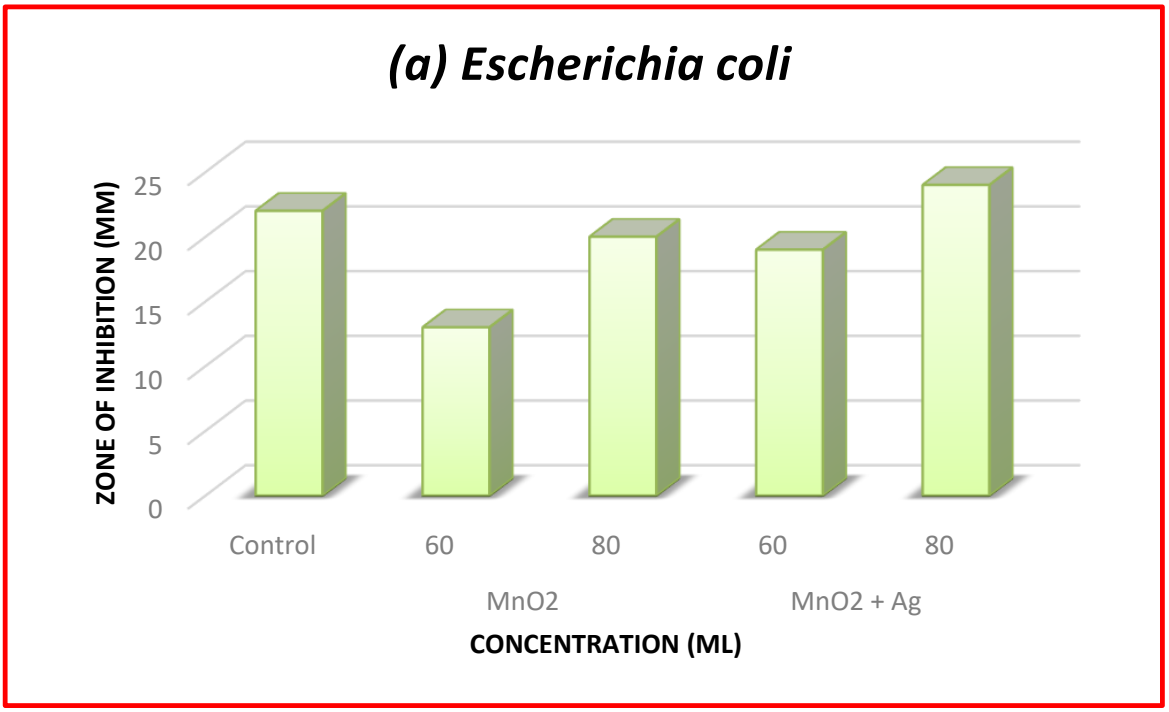


Figure 11. *Cont.*

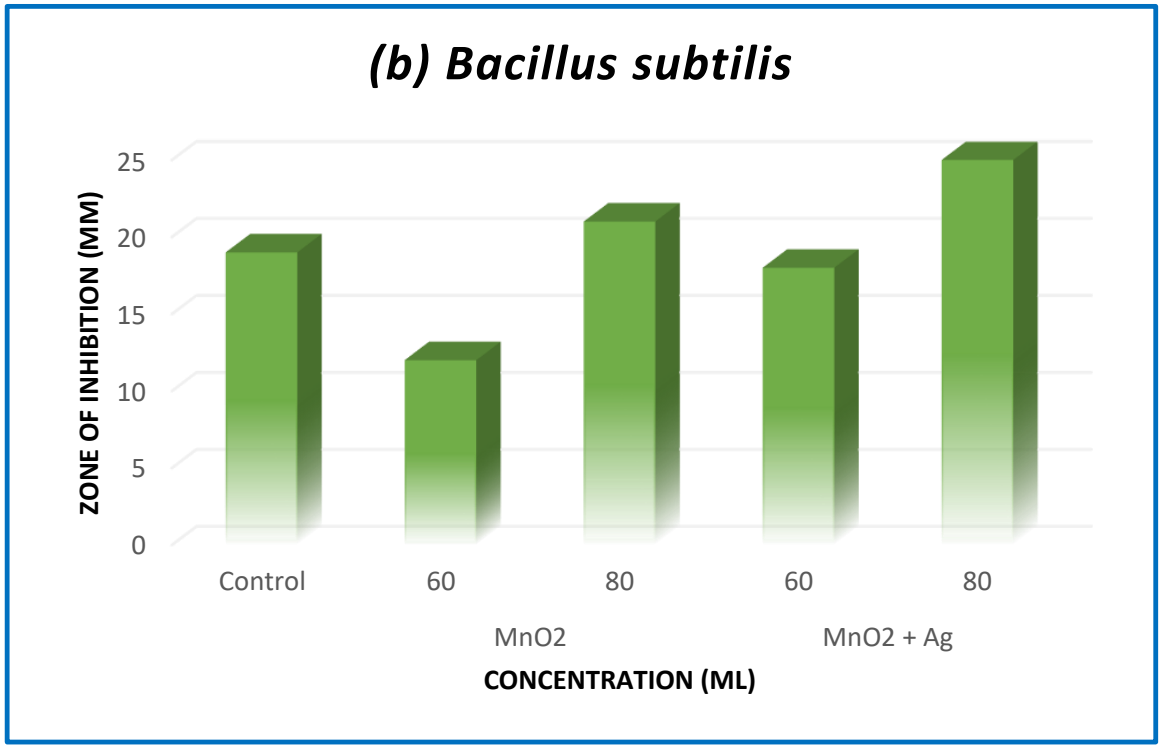


Figure 11. Zone of inhibition of MnO_2 doped with Ag nanoparticles against (**a**) Gram-negative (*Escherichia Coli*) bacteria and (**b**) Gram-positive strain (*Bacillus subtilis*).

2.7.2. Antifungal Activity

Fungi Tested

Two fungal strains (*Aspergillus niger and Candida albicans*) were used throughout the investigation. All the fungal cultures were obtained from the microbial type culture collection (MTCC), institute of microbial technology and Chandigarh, India. The young fungal broth cultures were prepared before the screening procedure. The agar well diffusion method was modified. Sabouraud's dextrose agar (SDA) was used for fungal cultures. The culture medium was inoculated with the fungal strains separately suspended in Sabouraud's dextrose broth. A total of 8 mm wells were punched into the agar and filled with plant extracts and solvent blanks (methanol, ethyl acetate and hexane). A standard antibiotic (Fucanazole, concentration 1 mg/mL) was used as a positive control, and fungal plates were incubated at 37 °C for 72 h. The diameters of the zones of inhibition observed were measured, as shown in Figure 12a,b. The sizes of the inhibitory zones that were detected were measured, as shown in Figure 13a,b. MnO_2 nanoparticles show good antifungal action against the C-albicans fumiga bacterium, according to the findings. The ability of silver nanoparticles to give strong antifungal efficacy was validated, indicating that MnO_2 nanoparticles has high potential activity, as evidenced by the zone of inhibition with the growth of tested bacteria, as shown in Table 1. The findings suggest that oxide nanoparticles containing metals like Ag could be helpful in the creation of antimicrobial agents [52].

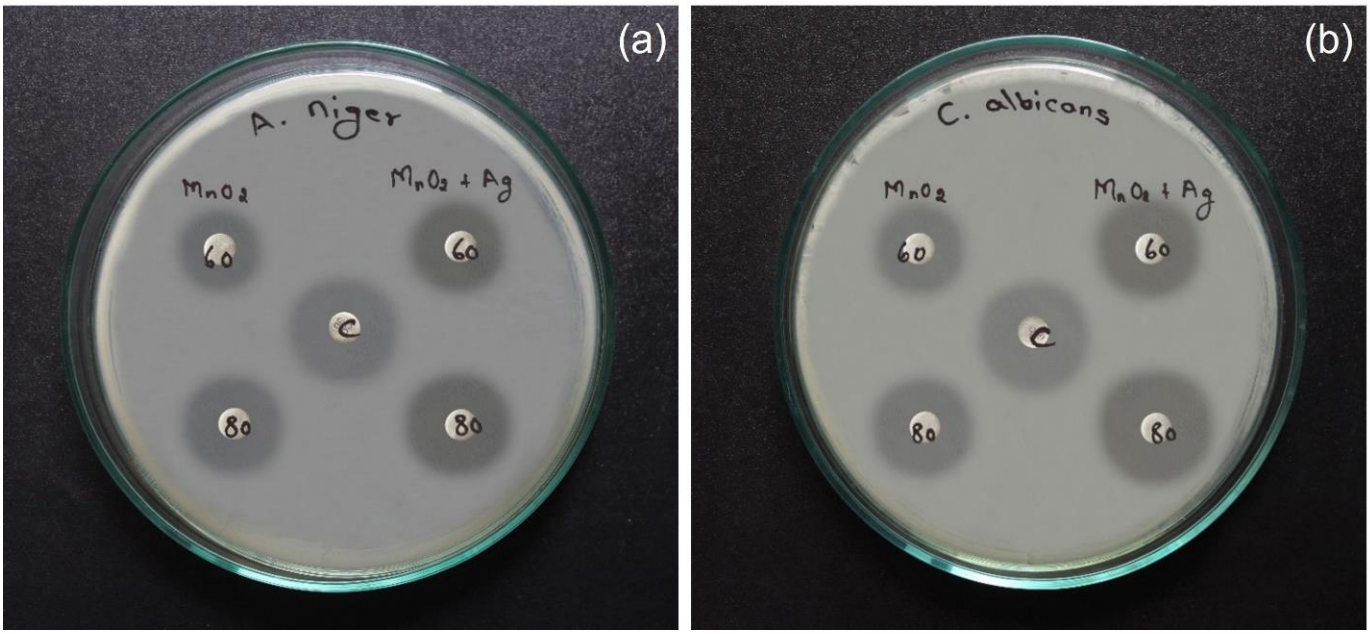


Figure 12. (**a**,**b**). Antifungal activity of MnO_2 doped with Ag nanoparticles against *Aspergillus niger and Candida albicans* stains.

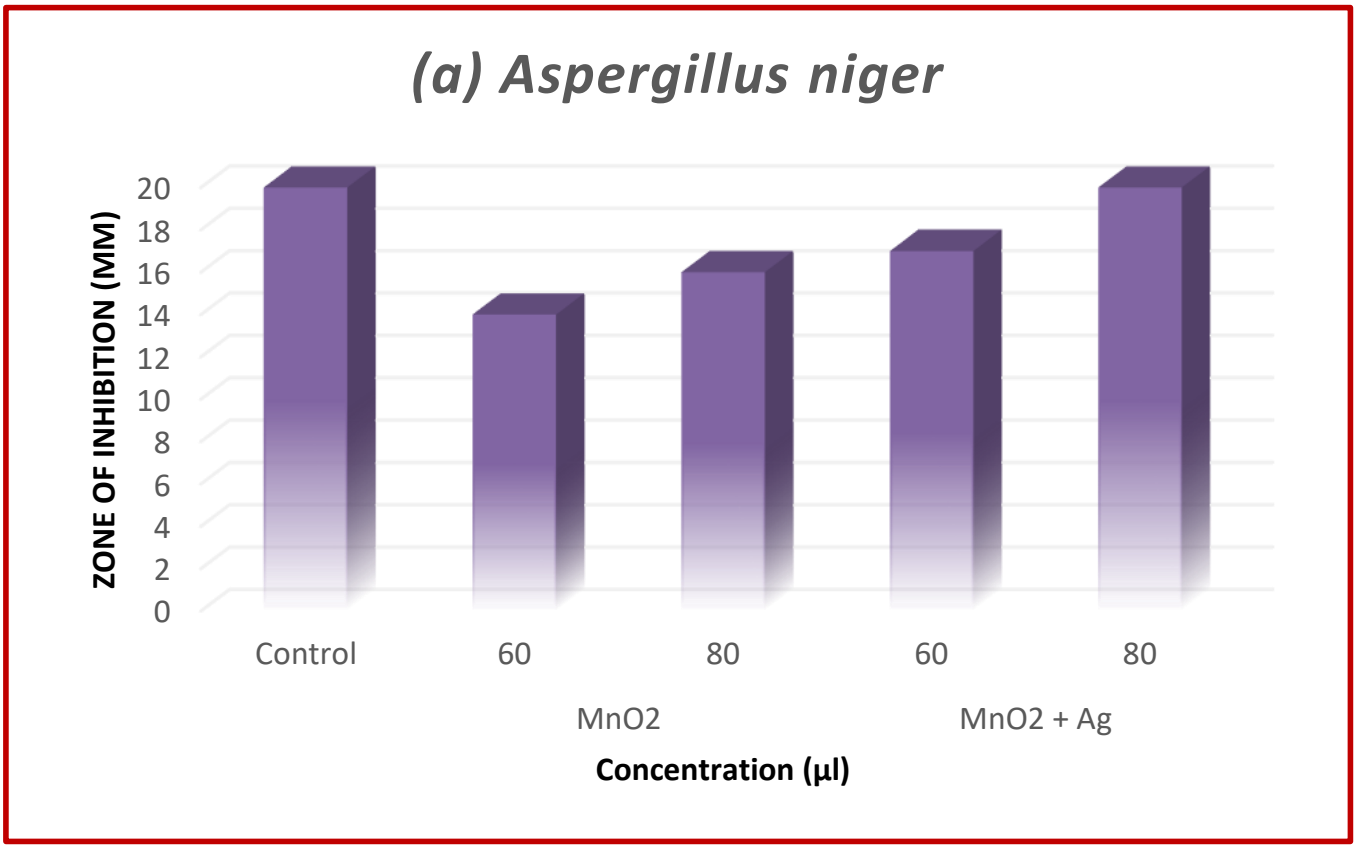


Figure 13. *Cont*.

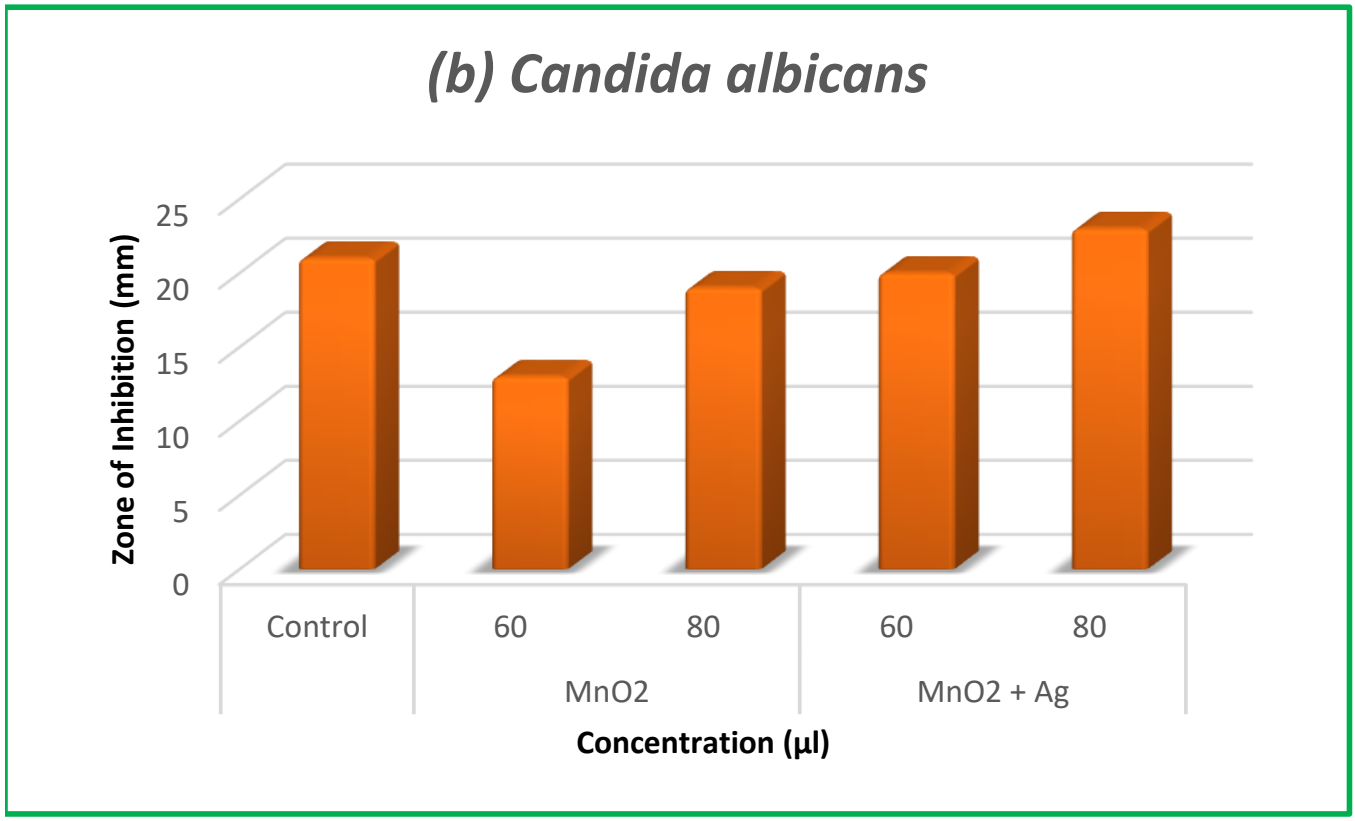


Figure 13. Zone of inhibition of MnO_2 doped with Ag nanoparticles against (**a**) *Aspergillus niger and* (**b**) *Candida albicans* stains.

Table 1. Antibacterial and Antifungal activity of $MnO_{2\ \text{doped with Ag}}$ against *Escherichia coli*, *Bacillus subtilis*, *Aspergillus niger* and *Candida albicans* strains.

Organism's	Control	Concentration (%)			
		Pure MnO_2		$MnO_{2\ \text{doped with Ag}}$	
		60	80	60	80
Bacillus subtilis	19	12	21	18	25
Escherichia coli	22	13	20	19	24
Aspergillus niger	20	14	16	17	20
Candida albicans	21	13	19	20	23

3. Experimental Methods

MnO_2 doped with Ag nanoparticles was made utilizing [$MnSO_4 \cdot H_2O$], $AgNO_3$, and $KMnO_4$ as raw materials in a straightforward sol–gel technique. [$MnSO_4 \cdot H_2O$] (0.9 g) was first dissolved in water (25 mL) using a sonicator. The aqueous dispersion of $KMnO_4$ (1.25 mg/mL) was then added to the solution under magnetic stirring. To make a gel, five percent $AgNO_3$ was added to the MnO_2 precursor and agitated for 8 h at 90 °C. The gel was then dried at 60 °C in a vacuum oven for later use. Finally, grey-hued MnO_2 doped with Ag nanoparticles was created. Pure MnO_2 was created using the same experimental method. All prepared samples were placed in an alumina crucible with a cover and cooked in a muffle furnace for 5 h at 500 °C. Fine nanoparticles of bare MnO_2 doped with Ag nanoparticles were collected and analysed.

3.1. Characterisation Studies

The sample was characterised by X-ray diffraction (Brucker D8 Advance) with CuKα radiation (λ = 1.5481 nm) with 2θ range from 10° to 90° at a scanning rate 10 deg/min to confirm the crystalline structure and to measure the particle size. A double beam UV–vis–NIR spectrometer was used to analyse the absorption properties of the prepared samples (Model No. UH5300). It was verified that moieties existed using an FTIR Spectrophotometer (SHIMADZU, 8400S). An optical Raman spectrometer (STR 300, AIRIX, Japan) was used to collect Raman spectrums with a diode laser source of 352 nm wavelength. For the surface morphology analysis, a scanning electron microscope (FESEM) (Carl Zeiss (ZEISS, Sigma)) was used, and for elemental analysis, an energy dispersive X-ray spectrometer (EDS) was used.

3.2. Photocatalytic Dye Degradation Test

When visible light was used to break down methylene blue (MB), the photocatalytic abilities of the photocatalysts were checked. One of the lights was a 500 W halogen lamp that can make visible light (λ > 420 nm) that can be seen by the people who are in the background. Fifty milligrams of the as-made photocatalysts added to 100 mL of water with constant magnetic stirring and water circulation. There were no lights or ventilation for 30 min. This allowed the adsorption and desorption equilibrium of MB on the photocatalysts to be reached. Then, the light was turned on. At 30-min intervals, 5 mL of the suspension was taken and centrifuged at 6000 rpm to remove the remaining photocatalyst. Then, the UV-vis spectrometer was used to look at the results. The decrease in the intensity of the characteristic band absorption at 662 nm was used to figure out how much MB had changed. The rate at which MB dyes break down when exposed to sunlight was determined by keeping track of the amount of withdrawn solutions absorbed at different times, λ_{max}~662 nm.

$$\text{Dyedegradationefficiency}(\%) = \frac{C_0 - C_t}{C_0} \times 100$$

C_o is the concentration at the start of the reaction, and C_t is the concentration at the time of the reaction.

4. Conclusions

In the present work, pure and doped MnO_2 nanoparticles were synthesised using a sol–gel process and were characterised using XRD, UV-vis, FTIR, SEM, EDX, Raman spectroscopy, photocatalytic studies, and with respect to antimicrobial activity. According to the XRD data, rhombohedral phase structures with crystalline sizes of 19.3 and 20.4 nm were formed. Optical analysis was used to determine the bandgap energies of MnO_2 nanostructures, which were determined to be 2.79 eV and 2.66 eV, respectively. FTIR and Raman spectroscopy shows the confined functional groups of pure and doped synthesised materials. The crystalline diameters were 80–90 nm, as determined by SEM and EDX. The photocatalytic characteristics of MB dye were investigated for MnO_2 doped with Ag, after 180 min, the degradation efficiency was assessed to be 90%, providing evidence that the created nanomaterials could potentially serve as good nanophotocatalysts. Even after five cycles of degradation testing, the cyclic degradation study revealed that nanoparticles were more stable. Pure and doped MnO_2 nanoparticles were found to obtain vigorous antibacterial activity against *E. coli* (Gram-negative bacteria) and *Bacillus subtilis* (Gram-positive bacteria) and a more potential antifungal activity against *Aspergillus niger* and *Candida albicans*. The synthesised MnO_2 doped with Ag nanoparticles shows that low-toxicity metal oxide nanoparticles could be widely used to eradicate a range of infectious diseases shortly. They could be employed as effective antibacterial, anticancer, and antioxidant agents in commercial biomedical applications, according to the findings.

Author Contributions: G.A.: Investigation, Original draft, Software, Data analysis, Writing—Review and Editing; R.A.K.: Formal analysis, Methodology, supervisor; Software and Visualisation; C.I.: Visualisation, Editing, Data analysis, Writing and Formal analysis; R.U.: Formal analysis, Software, Methodology and Visualisation; M.S.E.: Visualisation, Formal analysis, Software, Data management, Writing—Review and Editing; S.M.A.: Project administration, Funding acquisition, Data analysis, Visualisation, Writing, Review and Editing; K.K.: Validation, Project administration, Methodology, Investigation, Original draft, Supervisor; Visualisation; Writing, Review and Editing. All authors have read and agreed to the published version of the manuscript.

Funding: This research received no external funding.

Data Availability Statement: The datasets generated during and/or analysed during the current study are available from the corresponding author on reasonable request.

Acknowledgments: The authors gratefully acknowledge research funding from UNESCO-UNISA Africa Chair in Nanosciences/Nanotechnology Laboratories, College of Graduate Studies, University of South Africa (UNISA), Muckleneuk Ridge, Pretoria, South Africa. Additionally, this work was supported by the Distinguished Scientist Fellowship Program (DSFP) at King Saud University, Riyadh, Saudi Arabia.

Conflicts of Interest: The authors declare that they have no competing interest.

References

1. Magdalane, C.M.; Priyadharsini, G.M.A.; Kaviyarasu, K.; Jothi, A.I.; Simiyon, G.G. Synthesis and characterization of TiO_2 doped cobalt ferrite nanoparticles via microwave method: Investigation of photocatalytic performance of Congo red degradation dye. *Surf. Interfaces* **2021**, *25*, 101296. [CrossRef]
2. Lin, J.; Song, T.; Liu, Z.; Yang, D.; Xiang, R.; Hua, W.; Wan, H. Effects of biodegradable biomedical porous MnO_2 nanoparticles on blood components and functions. *Colloids Surf. B Biointerfaces* **2022**, *217*, 112667. [CrossRef] [PubMed]
3. Hosseinzadeh, M.; Mozaffari, S.A.; Ebrahimi, F. Porous 3D-graphene functionalized with MnO_2 nanospheres and NiO nanoparticles as highly efficient electrodes for asymmetric capacitive deionization: Evaluation by impedance-derived capacitance spectroscopy. *Electrochim. Acta* **2022**, *427*, 140844. [CrossRef]
4. Song, X.; Chen, X.; Liang, Z.; Xu, D.; Liang, Y. Colorimetric determination of Hg(II) ions based on core/shell Au@MnO_2 nanoparticles with oxidase-like activity. *J. Mol. Struct.* **2022**, *1263*, 133189. [CrossRef]
5. Renuka, R.; Devi, K.R.; Sivakami, M.; Thilagavathi, T.; Uthrakumar, R.; Kaviyarasu, K. Biosynthesis of silver nano particles using phyllanthus emblica fruit extract for antimicrobial application. *Biocatal. Agric. Biotechnol.* **2020**, *24*, 101567. [CrossRef]
6. Cui, Y.; Yang, K.; Lyu, Y.; Liu, P.; Zhang, Q.; Zhang, B. Hollow nitrogen-doped carbon nanofibers filled with MnO_2 nanoparticles/nanosheets as high-performance microwave absorbing materials. *Carbon* **2022**, *196*, 49–58. [CrossRef]
7. Wang, H.; Liang, Z.; Liu, C.; Zhu, L.; Xu, Y.; Zhou, L.; Yan, B. Construction of K and Tb Co-doped MnO_2 nanoparticles for enhanced oxidation and detoxication of organic dye waste. *Chemosphere* **2022**, *297*, 134104. [CrossRef]
8. Yuan, M.; Luo, F.; Rao, Y.; Yu, J.; Wang, Z.; Li, H.; Chen, X. SWCNT-bridged laser-induced graphene fibers decorated with MnO_2 nanoparticles for high-performance flexible micro-supercapacitors. *Carbon* **2021**, *183*, 128–137. [CrossRef]
9. Lam, S.M.; Lim, C.L.; Sin, J.C.; Zeng, H.; Lin, H.; Li, H. Facile synthesis of MnO_2/ZnO coated on cotton fabric for boosted antimicrobial, self-cleaning and photocatalytic activities under sunlight. *Mater. Lett.* **2021**, *305*, 130818. [CrossRef]
10. Logambal, S.; Maheswari, C.; Chandrasekar, S.; Thilagavathi, T.; Inmozhi, C.; Panimalar, S.; Bassyouni, F.; Uthrakumar, R.; Gawwad, M.R.A.; Aljowaie, R.M.; et al. Synthesis and characterizations of CuO nanoparticles using *Couroupita guianensis* extract for and antimicrobial applications. *J. King Saud Univ.-Sci.* **2022**, *34*, 101910. [CrossRef]
11. Vimuna, V.M.; Raj, B.B.; Sam, S.C.; Xavier, T.S. One-pot temperature-controlled hydrothermal synthesis of α-MnO_2 nanoparticles decorated thermally reduced graphene oxide composite as high-performance flexible aqueous symmetric supercapacitors. *Diam. Relat. Mater.* **2021**, *120*, 108707. [CrossRef]
12. Kumar, S.; Choudhary, R.B. Influence of MnO_2 nanoparticles on the optical properties of polypyrrole matrix. *Mater. Sci. Semicond. Process.* **2022**, *139*, 106322. [CrossRef]
13. Lian, Y.; Yuan, X.; Wang, Y.; Wei, L. Highly sensitive visual colorimetric sensor for xanthine oxidase detection by using MnO_2-nanosheet-modified gold nanoparticles. *Spectrochim. Acta Part A Mol. Biomol. Spectrosc.* **2022**, *276*, 121219. [CrossRef] [PubMed]
14. George, A.; Raj, D.M.A.; Venci, X.; Raj, A.D.; Irudayaraj, A.A.; Josephine, R.L.; Sundaram, S.J.; Al-Mohaimeed, A.M.; Al Farraj, D.A.; Chen, T.W.; et al. Photocatalytic effect of CuO nanoparticles flower-like 3D nanostructures under visible light irradiation with the degradation of methylene blue (MB) dye for environmental application. *Environ. Res.* **2022**, *203*, 111880. [CrossRef]
15. Aadil, M.; Mahmood, M.; Warsi, M.F.; Alsafari, I.A.; Zulfiqar, S.; Shahid, M. Fabrication of MnO_2 nanowires and their nanohybrid with flat conductive matrix for the treatment of industrial effluents. *Flatchem* **2021**, *30*, 100316. [CrossRef]
16. Panimalar, S.; Logambal, S.; Thambidurai, R.; Inmozhi, C.; Uthrakumar, R.; Muthukumaran, A.; Rasheed, R.A.; Gatasheh, M.K.; Raja, A.; Kennedy, J.; et al. Effect of Ag doped MnO_2 nanostructures suitable for wastewater treatment and other environmental pollutant applications. *Environ. Res.* **2022**, *205*, 112560. [CrossRef]

17. Saini, A.K.; Sahoo, S.K. Fluorescent pH sensing and MnO_2 nanosphere directed turn-on sensing of glutathione using pyridoxal 5′-phosphate modified polydopamine nanoparticles. *Inorg. Chem. Commun.* **2022**, *142*, 109677. [CrossRef]
18. Mohan, V.; Marappan, G.; Chidambaram, D.; Rajendran, K.; Surya, V.J.; Venugopal, G.; Sivalingam, Y. Photo-enhanced acetone adsorption on δ-MnO_2 nanoparticles: A step towards non-invasive detection of diabetes mellitus. *Mater. Lett.* **2022**, *306*, 130944. [CrossRef]
19. Deng, Y.; Chen, Z.; Huang, J.; Yang, G.; Zhang, Q.; Liu, Z.; Cao, Y.; Peng, F. MnO_2 nanoparticles supported on CNTs for cumene oxidation: Synergistic effect and kinetic modelling. *Chem. Eng. J.* **2022**, *444*, 136666. [CrossRef]
20. Wang, L.; He, H.; Zhang, C.; Sun, L.; Liu, S.; Wang, S. Antimicrobial activity of silver loaded MnO_2 nanomaterials with different crystal phases against Escherichia coli. *J. Environ. Sci.* **2016**, *41*, 112–120. [CrossRef]
21. Panimalar, S.; Subash, M.; Chandrasekar, M.; Uthrakumar, R.; Inmozhi, C.; Al-Onazi, W.A.; Al-Mohaimeed, A.M.; Chen, T.W.; Kennedy, J.; Maaza, M.; et al. Reproducibility and long-term stability of Sn doped MnO_2 nanostructures: Practical photocatalytic systems and wastewater treatment applications. *Chemosphere* **2022**, *293*, 133646. [CrossRef] [PubMed]
22. Geetha, N.; Sivaranjani, S.; Ayeshamariam, A.; Siva Bharathy, M.; Nivetha, S.; Kaviyarasu, K.; Jayachandran, M. High performance photo-catalyst based on nanosized ZnO-TiO_2 nanoplatelets for removal of RhB under visible light irradiation. *J. Adv. Microsc. Res.* **2018**, *13*, 12–19. [CrossRef]
23. Wang, S.; Zheng, H.; Zhou, L.; Cheng, F.; Liu, Z.; Zhang, H.; Zhang, Q. Injectable redox and light responsive MnO_2 hybrid hydrogel for simultaneous melanoma therapy and multidrug-resistant bacteria-infected wound healing. *Biomaterials* **2020**, *260*, 120314. [CrossRef] [PubMed]
24. Alhaji, N.M.I.; Nathiya, D.; Kaviyarasu, K.; Meshram, M.; Ayeshamariam, A. A comparative study of structural and photocatalytic mechanism of $AgGaO_2$ nanocomposites for equilibrium and kinetics evaluation of adsorption parameters. *Surf. Interfaces* **2019**, *17*, 100375. [CrossRef]
25. Gogoi, N.; Babu, P.J.; Mahanta, C.; Bora, U. Green synthesis and characterization of silver nanoparticles using alcoholic flower extract of Nyctanthesarbortristis and in vitro investigation of their antibacterial and cytotoxic activities. *Mater. Sci. Eng.* **2015**, *46*, 463–469. [CrossRef] [PubMed]
26. Liu, S.; Ma, J.; Wang, S.; Chen, S.; Wang, B.; Li, J. nanoparticles incorporated Chitosan/calcium pyrophosphate hybrid micro flowers for antibacterial applications. *Mater. Lett.* **2019**, *255*, 126570. [CrossRef]
27. Wu, W.; Wu, Z.; Yu, T.; Jiang, C.; Kim, W.-S. Recent progress on magnetic iron oxide nanoparticles: Synthesis, surface functional strategies and biomedical applications. *Sci. Technol. Adv. Mater.* **2015**, *16*, 023501. [CrossRef]
28. George, A.; Raj, A.D.; Irudayaraj, A.A.; Josephine, R.L.; Venci, X.; Sundaram, S.J.; Rajakrishnan, R.; Kuppusamy, P.; Kaviyarasu, K. Regeneration study of MB in recycling runs over nickel vanadium oxide by solvent extraction for photocatalytic performance for wastewater treatments. *Environ. Res.* **2022**, *211*, 112970. [CrossRef]
29. Maddila, S.N.; Maddila, S.; Bhaskaruni, S.V.; Kerru, N.; Jonnalagadda, S.B. MnO_2 on hydroxyapatite: A green heterogeneous catalyst and synthesis of pyran-carboxamide derivatives. *Inorg. Chem. Commun.* **2020**, *112*, 107706. [CrossRef]
30. Perumal, V.; Inmozhi, C.; Uthrakumar, R.; Robert, R.; Chandrasekar, M.; Mohamed, S.B.; Honey, S.; Raja, A.; Al-Mekhlafi, F.A.; Kaviyarasu, K. Enhancing the photocatalytic performance of surface—Treated SnO2 hierarchical nanorods against methylene blue dye under solar irradiation and biological degradation. *Environ. Res.* **2022**, *209*, 112821. [CrossRef]
31. Patra, T.; Mohanty, A.; Singh, L.; Muduli, S.; Parhi, P.K.; Sahoo, T.R. Effect of calcination temperature on morphology and phase transformation of MnO_2 nanoparticles: A step towards green synthesis for reactive dye adsorption. *Chemosphere* **2022**, *288*, 132472. [CrossRef]
32. Qu, Y.; Zheng, X.; Ma, K.; He, W.; Wang, S.; Zhang, P. Facile coating of MnO_2 nanoparticles onto polymer fibers via friction-heating adhesion for efficient formaldehyde removal. *Chem. Eng. J.* **2022**, *430*, 132954. [CrossRef]
33. Kouotou, P.M.; Vieker, H.; Tian, Z.Y.; Ngamou, P.H.T.; El Kasmi, A.; Beyer, A.; Gölzhäuser, A.; Kohse-Höinghaus, K. Structure–activity relation of spinel-type Co–Fe oxides for low-temperature CO oxidation. *Catal. Sci. Technol.* **2014**, *4*, 3359–3367. [CrossRef]
34. Al-Thubaiti, K.S.; Khan, Z.; Al-Thabaiti, S.A. Effects of CTAB and SDS on the nucleation and growth of MnO_2 and Ag-doped MnO_2 nanoparticles formation. *J. Mol. Liq.* **2022**, *355*, 118910. [CrossRef]
35. Shannon, R.D. Revised Effective Ionic Radi and systematic studies of interatomic Distance in Halides and chaleogenides. *Acta Crystallogr.* **1976**, *32*, 751–767. [CrossRef]
36. Panimalar, S.; Uthrakumar, R.; Selvi, E.T.; Gomathy, P.; Inmozhi, C.; Kaviyarasu, K.; Kennedy, J. Studies of MnO_2/g-C_3N_4 hetrostructure efficient of visible light photocatalyst for pollutants degradation by sol-gel technique. *Surf. Interfaces* **2020**, *20*, 100512. [CrossRef]
37. Dong, X.; Wang, X.; Wang, J.; Song, H.; Li, X.; Wang, L.; Chan-Park, M.; Li, C.M.; Chen, P. Synthesis of a MnO_2–graphene foam hybrid with controlled MnO_2 particle shape and its use as a supercapacitor electrode. *Carbon* **2012**, *50*, 4865–4870. [CrossRef]
38. Manjula, N.; Kaviyarasu, K.; Ayeshamariam, A.; Selvan, G.; Diallo, A.; Ramalingam, G.; Mohamed, S.B.; Letsholathebe, D.; Jayachandran, M. Structural, morphological and methanol sensing properties of jet nebulizer spray pyrolysis effect of TiO_2 doped SnO_2 thin film for removal of heavy metal ions. *J. Nanoelectron. Optoelectron.* **2018**, *13*, 1543–1551. [CrossRef]
39. Mollaei, Z.; Kermani, F.; Moosavi, F.; Kargozar, S.; Khakhi, J.V.; Mollazadeh, S. In silico study and experimental evaluation of the solution combustion synthesized manganese oxide (MnO_2) nanoparticles. *Ceram. Int.* **2022**, *48*, 1659–1672. [CrossRef]
40. Xu, R.; Wang, Z.; Gao, L.; Wang, S.; Zhao, J. Effective design of MnO_2 nanoparticles embedded in laser-induced graphene as shape-controllable electrodes for flexible planar micro supercapacitors. *Appl. Surf. Sci.* **2022**, *571*, 151385. [CrossRef]

41. Cao, M.; Zhuang, Z.; Liu, Y.; Zhang, Z.; Xuan, J.; Zhang, Q.; Wang, W. Peptide-mediated green synthesis of the MnO_2@ZIF-8 core–shell nanoparticles for efficient removal of pollutant dyes from wastewater via a synergistic process. *J. Colloid Interface Sci.* **2022**, *608*, 2779–2790. [CrossRef]
42. Arularasu, M.V.; Anbarasu, M.; Poovaragan, S.; Sundaram, R.; Kanimozhi, K.; Magdalane, C.M.; Kaviyarasu, K.; Thema, F.T.; Letsholathebe, D.; Mola, G.T.; et al. Structural, optical, morphological, and microbial studies on SnO_2 nanoparticles prepared by co-precipitation method. *J. Nanosci. Nanotechnol.* **2018**, *18*, 3511–3517. [CrossRef] [PubMed]
43. Ding, D.; Zhou, Y.; He, T.; Rong, S. Facet selectively exposed α-MnO_2 for complete photocatalytic oxidation of carcinogenic HCHO at ambient temperature. *Chem. Eng. J.* **2022**, *431*, 133737. [CrossRef]
44. Panimalar, S.; Chandrasekar, M.; Logambal, S.; Uthrakumar, R.; Inmozhi, C. Europium-doped MnO_2 nanostructures for controlling optical properties and visible light photocatalytic activity. *Mater. Today Proc.* **2022**, *56*, 3394–3401. [CrossRef]
45. Xie, C.; Xu, L.; Xia, Y.; Gang, R.; Ye, Q.; Koppala, S. Evaluation of visible photocatalytic performance of microwave hydrothermal synthesis of MnO_2/TiO_2 core-shell structures and gaseous mercury removal. *Microporous Mesoporous Mater.* **2022**, *334*, 111788. [CrossRef]
46. Chandrasekar, M.; Subash, M.; Perumal, V.; Panimalar, S.; Aravindan, S.; Uthrakumar, R.; Inmozhi, C.; Isaev, A.B.; Muniyasamy, S.; Raja, A.; et al. Specific charge separation of Sn doped MgO nanoparticles for photocatalytic activity under UV light irradiation. *Sep. Purif. Technol.* **2022**, *294*, 121189. [CrossRef]
47. Khatri, M.; Gupta, A.; Gyawali, K.; Adhikari, A.; Koirala, A.R.; Parajuli, N. Photocatalytic degradation of dyes using synthesized δ-MnO_2 nanostructures. *Chem. Data Collect.* **2022**, *39*, 100854. [CrossRef]
48. Bahiraei, A.; Behin, J. Sonochemical immobilization of MnO_2 nanoparticles on NaP-zeolite for enhanced Hg (II) adsorption from water. *J. Environ. Chem. Eng.* **2020**, *8*, 103790. [CrossRef]
49. Perumal, V.; Sabarinathan, A.; Chandrasekar, M.; Subash, M.; Inmozhi, C.; Uthrakumar, R.; Isaev, A.B.; Raja, A.; Elshikh, M.S.; Almutairi, S.M.; et al. Hierarchical nanorods of graphene oxide decorated SnO_2 with high photocatalytic performance for energy conversion applications. *Fuel* **2022**, *324*, 124599. [CrossRef]
50. Shoba, A.; Kavitha, B.; Aswathaman, H.; Ganesan, H.; Kumar, N.S. Synthesis, characterization and electrochemical sensors application of MnO_2 nanoparticles. *Mater. Today Proc.* **2022**, *48*, 521–526. [CrossRef]
51. Yu, W.; Liu, T.; Cao, S.; Wang, C.; Chen, C. Constructing MnO_2/single crystalline ZnO nanorod hybrids with enhanced photocatalytic and antibacterial activity. *J. Solid-State Chem.* **2016**, *239*, 131–138. [CrossRef]
52. Rahmat, M.; Bhatti, H.; Rehman, A.; Chaudhry, H.; Yameen, M.; Iqbal, M.; Al-Mijalli, S.; Alwadai, N.; Fatima, M.; Abbas, M. Bionanocomposite of Au decorated MnO_2 via in situ green synthesis route and antimicrobial activity evaluation. *Arab. J. Chem.* **2021**, *14*, 103415. [CrossRef]

Disclaimer/Publisher's Note: The statements, opinions and data contained in all publications are solely those of the individual author(s) and contributor(s) and not of MDPI and/or the editor(s). MDPI and/or the editor(s) disclaim responsibility for any injury to people or property resulting from any ideas, methods, instructions or products referred to in the content.